JOURNAL OF MATERIALS SCIENCE 27 (1992) 6452–6462

The influence of mixing on the microstructure of the cement paste/aggregate interfacial zone and on the strength of mortar

ALAN W. POPE, HAMLIN M. JENNINGS*
*Department of Materials Science and Engineering, *and also Department of Civil Engineering, Northwestern University, 2145 Sheridan Road, Evanston, IL 60208, USA*

The influence of mixing on the microstructure of the cement paste/aggregate bond has been investigated. Back-scattered electron microscopy was used in conjunction with quantitative image analysis to examine the microstructure of the interface between limestone aggregate and the cement matrix in a series of mortars. The distribution of porosity and anhydrous material along the paste/aggregate interface was shown to be dependent upon the relative abundance of water at the aggregate surface during mixing. Improvements in the interfacial microstructure were shown to correlate with improvements in strength and fracture properties. The interfacial zones seen in the limestone mortars were compared with a model interfacial system. A new classification system for two types of interfacial regions in mortar is proposed.

1. Introduction

Cement paste, while frequently studied as an independent material, is almost always used as the matrix component of a composite material reinforced with aggregate. The performance of this composite depends on the mechanical and chemical bonding of the matrix and its second phase. Also, the role of the interface between the cement matrix and aggregate has become the subject of numerous studies and literature reviews detailing the microstructural development of this area, and the resulting mechanical effects this development has on the mechanical properties of the concrete system [1–7].

Farran and co-workers [8–10] were the first to describe the region surrounding a reinforcing phase as an "aureole de transition", approximately 50 μm thick where the traditional hydration products of cement were less dense than in the bulk paste. Later, Hadley [11] and then Barnes and co-workers [12–13] expanded the understanding of the transition area by using scanning electron microscopy in conjunction with an X-ray spectrometer to describe the interfacial region between glass slides or quartz and cement paste. They proposed the following path of microstructural development.

(i) A thin film of calcium hydroxide (CH) is deposited with its *c*-axis perpendicular to the surface of the aggregate.

(ii) The film is covered with a layer of elongated calcium silicate hydrate (C–S–H) particles.

(iii) Larger CH crystals precipitate with their *c*-axis parallel to the surface of the aggregate.

(iv) Additional, space-filling CH crystals form near the interface [14].

The two-layer or duplex film originally described by Barnes has been recognized in other paste/aggregate and paste/fibre systems [15–19], but a number of researchers have found no evidence of such a film [20–22]. Scrivener and Gartner [23] proposed a possible resolution to these conflicting results by suggesting that the film is linked to the polished surfaces used in systems that model the paste/aggregate interface. In other words, water films, like those described by Maso [18], may form more easily on polished surfaces and then contribute to the diffusion of ions along the interface, where poor particle packing leaves room for hydration products to nucleate and grow [2, 6].

The interfacial zone is also thought to be rich in CH and ettringite. Quantitative X-ray diffraction (QXRD) studies using the technique developed by Grandet and Ollivier [24] indicate that concentrations of CH and ettringite increase as the interface is approached from the bulk paste [15, 16]. In this technique, successive layers of the interfacial zone are removed by abrasion for analysis with XRD. Concentration and orientation information for crystalline hydration products is attained as a function of the distance from the interface. This technique has shown that CH is oriented with its *c*-axis parallel to the aggregate surface, but this orientation decreases with increasing distance from the aggregate surface [25]. While research utilizing secondary electron imaging (SEI) of fracture surfaces [11–13] supports the contention that greater amounts of CH and ettringite exist in the interfacial region, other studies using quantitative back-scattered electron imaging (BEI) of the paste/aggregate interface conclude that no such increase exists, except in those

0022–2461

regions where bleeding is likely to occur [20–23]. However, fracture surfaces may have unrepresentative concentrations of CH due to the inherent weakness of the crystals along their basal plane [22]. Gartner proposed that the discrepancy in the XRD and BSE determined CH concentrations is the result of XRD being a mass-weighted analytical technique while BSE is a volume-weighted analytical technique. By making certain assumptions about the density of the C–S–H gel in the interfacial region, he converted BEI-derived volume distribution data to mass fractions, which agree with the XRD analytical measurements [26].

Another important characteristic of the interfacial region is the concentration of porosity near the interface. Previous research [2, 23, 27] has shown that anhydrous materials pack poorly along the interface, leading to localized high water to cement (w/c) ratios. This appears to increase capillary porosity and the concentration of hollow-shelled hydration grains, or Hadley grains. The concentration of these grains in the interfacial zone close to the aggregate surface, contributes to the large porosity gradients documented by Scrivener and Gartner [23].

1.1. Interfacial microstructure and the mechanical properties of cement composites

The bulk properties of a composite determine the type and extent of its use. Numerous studies indicate that the microstructure of the paste/aggregate interface greatly influences the mechanical properties of mortar and concrete. For example, Mindess and Diamond [28] and Maji and Shah [29] have found that cracking initiates in the interfacial zone and that the crack path propagates through this zone, just a few micrometres from the aggregate surface. Goldman and Bentur [30] showed the connection between the interfacial microstructure and strength improvement. They added an inert filler similar in size and shape to silica fume to a paste and a concrete made with an identical paste. The filler acted to reduce the size of the interfacial zone and resulted in a concrete with greater strength than its corresponding paste. Thus, a reduction in size of the paste/aggregate interfacial zone has a direct correlation to improved concrete strength.

The implications of the quality of the cement paste/aggregate interface on the strength of concrete have led to mixing processes designed to reduce the amount of water and increase the amount of anhydrous cement located adjacent to the aggregate surface. Xueqan *et al.* [31–33], Hayakawa and Itoh [34] and Higuchi [35] have shown that techniques incorporating a pre-coating of the aggregate with a lower w/c ratio slurry, yield improvements in strength because of an improved cement paste/aggregate bond. However, Xueqan *et al.*'s work also incorporated chemical pre-treatment of aggregate surfaces, thereby making it impossible to isolate the effects of pre-coating from those of chemical pre-treatment. Hayakawa and Itoh, and Higuchi used a pre-coating technique without chemical pre-treatment in their work, but they evaluated their results only in terms of its affects on mechanical properties.

This paper expands upon the research discussed above. Back-scattered electron microscopy is used in conjunction with quantitative image analysis to evaluate the effect of mixing on the microstructure of the paste/aggregate interface. This experimental programme characterizes both the mechanical properties and the interfacial microstructure of a series of limestone mortars. Two different model systems using polished limestone aggregates are also examined to illustrate the differences between the microstructure of model systems and that of normal cement composite systems.

2. Experimental procedure

2.1. Materials

The cement used in this study is a commercially available ASTM type I Portland cement. Its chemical and mineral compositions are shown in Tables I and II. The particle-size distribution of this cement, as determined by a laser diffraction particle size analyser, is shown in Table III. A dolomitic limestone aggregate from the McCook Quarry, McCook, IL, was used for all samples. The composition and particle-size distribution of the aggregate are shown in Tables IV and V. The aggregates used in the model test systems were cut from larger stones taken from the same quarry.

2.2. Mixing

A series of five limestone mortars were made with the main variables as shown in Table VI. Mixes labelled 1–3 incorporated varying amounts of pre-coating using a mixing procedure patterned after that of Xueqan *et al.* [31–33] and Hayakawa and Itoh [34]. The procedure consisted of four steps: (1) the mixing water is divided into two parts; (2) one part of the mixing water, Water 1, is mixed with the aggregates; (3) the cement is added to the wet aggregates and mixed for 5 min, forming a thick slurry and, (4) the second part of the water, Water 2, is added to the slurry/aggregate mixture and mixed to form a homogeneous fresh mortar. Mixes four and five used paste that was mixed separately in a large bench-top mixer and then added to the aggregate. All mixing of the mortar was done in a large rotary mixer. The water:cement:aggregate ratio by weight for all mixes was 0.45:1:2.5.

TABLE I Chemical composition of continental™ Type 1 Portland cement

Compound	%
Silicon dioxide, SiO_2	20.80
Aluminium oxide, Al_2O_3	5.00
Ferric oxide, Fe_2O_3	2.77
Calcium oxide, CaO	62.00
Magnesium oxide, MgO	4.50
Sulphur trioxide, SO_3	2.80
Sodium oxide equiv, Na_2O	0.60
Ignition loss	0.50
Insoluble residue	0.28

TABLE II Mineral composition of Continental™ Type 1 Portland cement

Compound	%
Tricalcium silicate C_3S	52.40
Dicalcium silicate, C_2S	20.11
Tricalcium aluminate, C_3A	8.60
Tetra calcium aluminoferrite, C_4AF	8.43

TABLE III Particle-size distribution of Continental™ Type 1 Portland cement

Cumulative per cent finer (%)	Particle size (mm)
90.00	35.10
75.00	23.61
50.00	11.15
25.00	4.05
10.00	1.10

TABLE IV Sieve analysis of aggregate

Sieve size	Percentage passing through sieve
3/8	100
4	97.0
8	71.0
16	49.0
40	31.0
50	28.0
100	23.0
200	19.0

TABLE V Chemical analysis of aggregate

Chemical compound	%
Calcium carbonate, $CaCO_3$	55.05
Magnesium carbonate, $MgCO_3$	49.90
Silicon dioxide, SiO_2	1.68
Aluminium oxide, Al_2O_3	0.20
Ferric oxide, Fe_2O_3	19.00

TABLE VI Mix proportions and mix times of experimental set (w/c = 0.45)

Mix	Water 1(%)	Water 2(%)	Aggregate	Cement	Mix time (min)
1	100	0	2.5	1	10 min
2	25	75	2.5	1	5/10
3	50	50	2.5	1	5/10
4	100	0	2.5	1	10, paste 5, mortar
5	100	0	2.5	1	10, paste 10, mortar

After mixing, the mortar was cast into 76.2 mm × 152.4 mm compression cylinders according to ASTM C192. Beams that were 25.4 mm wide, 76.2 mm tall, and 228.6 mm long were also cast and then vibrated for consolidation. A 16.9 mm notch was cast into each beam. All specimens were removed from the mould after 1 day and cured in saturated lime water at 25 °C for either 7 or 28 days. After 48 h, beams were cut to a height of 50.8 mm on a large band saw and then returned to the lime bath for the full duration of curing.

In addition to the five mortar mixes, two additional samples were made using paste cast against a polished aggregate. A 10 mm × 30 mm × 5 mm piece of aggregate was cut from a larger piece of dolomitic limestone on a diamond saw. One side of this aggregate was polished down to a 1/4 μm finish. In a small bench-top mixer, 300 g cement were mixed with 135 g water (w/c = 0.45) for 10 min. The paste was then cast against the polished surface. A second sample utilized smaller pieces of polished aggregate (5 mm × 5mm × 10 mm). Again, 300g cement were mixed with 135 g water for 10 min. At the end of this mixing, the pieces of polished aggregate were then added to the mixer and mixed with the paste for a further 5 min. The mixture of the cement paste and the polished aggregate was then cast into a small cylinder.

2.3. Mechanical characterization

For each mortar mix, four cylinders were prepared for compression tests and tested according to ASTM 39–86. Their results are shown in Fig. 1.

The two-parameter fracture model proposed by Jenq and Shah [36] was used to characterize the relative toughness and Young's modulus of the various mortar mixes. The procedure for the determination of the elastic modulus and the two fracture parameters in this model, the critical stress intensity factor, K_{Ic}^{s} and the crack tip opening displacement, $CTOD_c$, is described in detail elsewhere [37]. A closed-loop testing system was used for all fracture tests. The testing configuration and specimen geometry are shown in Fig. 2. The results of these tests are shown in Tables VII and VIII.

2.4. Microstructural sample preparation and evaluation

In order to quantify the microstructural gradients in these mortars, one 1 mm thick specimen was cut from each sample on a diamond saw at 7 and 28 days and mounted for evaluation with back-scattered electron imaging. After many experimental procedures

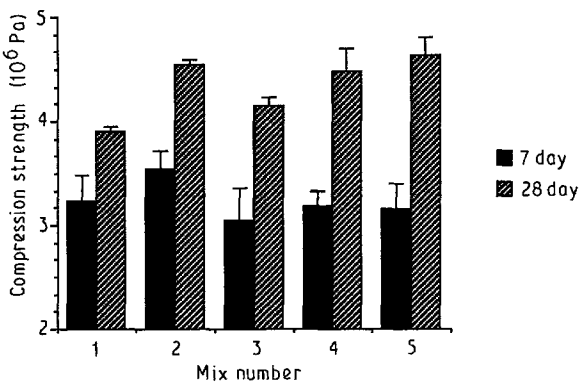

Figure 1 Compression strength values at 7 and 28 days hydration. Error bars denote 90% confidence intervals.

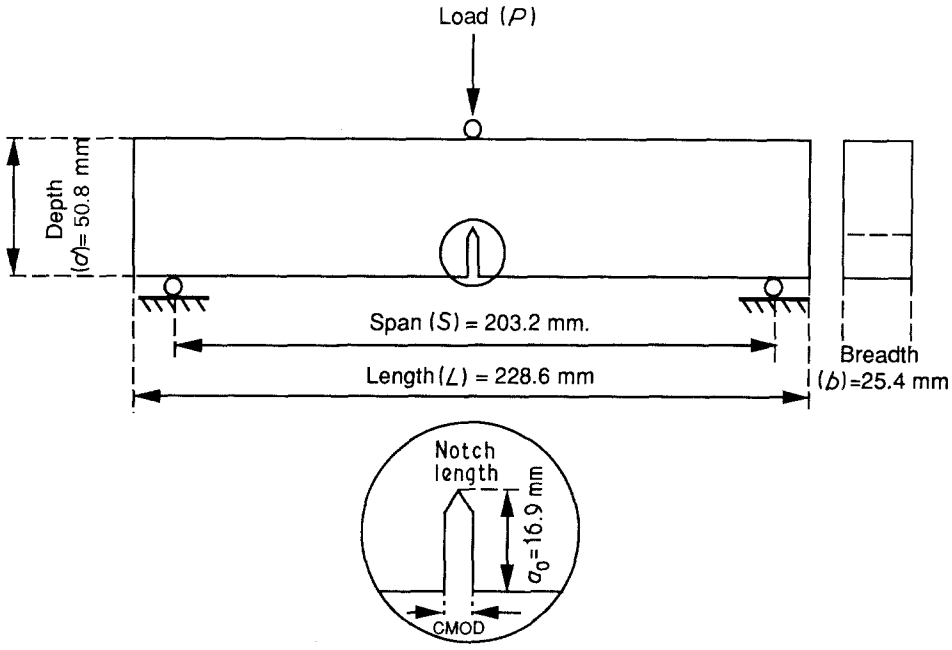

Figure 2 Testing configuration and specimen geometry for the two-parameter fracture model tests (36).

TABLE VII Fracture properties of limestone mortars (7 day)

Mix	Young's modulus (10^{10} Pa)	90% CI ± (10^9 Pa)	K^s_{Ic} ($Nm^{-3/2}$)	90% CI ± ($Nm^{-3/2}$)	$CTOD_c$ (μm)	90% CI ± (μm)	Critical crack A_c(m)
1	1.77	5.33	570 899.7	69 017.1	7.74	1.89	0.0220
2	2.12	1.36	594 878.1	50 128.9	5.90	0.523	0.0207
3	1.84	1.66	597 999.7	90 618.0	7.04	2.08	0.0211
4	1.97	1.64	517 998.1	47 051.5	5.36	0.282	0.0205
5	1.99	3.91	552 869.1	54 832.7	6.69	3.29	0.0208

TABLE VIII Fracture properties of limestone mortars (28 day)

Mix	Young's modulus (10^{10} Pa)	90% CI ± (10^9 Pa)	K^s_{Ic} ($Nm^{-3/2}$)	90% CI ± ($Nm^{-3/2}$)	$CTOD_c$ (μm)	90% CI ± (μm)	Critical crack A_c(m)
1	1.83	2.46	481 742.5	65 640.0	5.64	0.199	0.0208
2	2.19	1.36	579 566.4	36 870.0	5.21	0.194	0.0204
3	2.15	1.36	631 269.0	17 370.0	6.16	0.204	0.0208
4	2.20	1.23	615 689.3	100 200.0	5.11	2.26	0.0198
5	2.19	1.49	613 765.3	98 570.0	5.12	2.24	0.0200

were tried, it was determined that optimal contrast and minimum microstructural damage was obtained by mounting the samples according to the procedures developed by Struble and Stutzman [38]. This technique prevents drying damage and promotes optimum epoxy impregnation by gradually replacing water with ethanol followed by a replacement of ethanol with a low viscosity epoxy. Samples were then oven cured at 60° C for 24 h. Once mounted, samples were dry polished with 320 grit paper followed by 400 grit paper. Polishing then proceeded with 600 grit paper lubricated with a non-aqueous polishing lubricant. Lapp cloths impregnated with diamond pastes of 6, 3, 1 and 1/4 μm were used to bring the samples to a 1/4 μm polish.

The interfacial zone was examined with an environmental scanning electron microscope interfaced directly to an image analyser. The ESEM, described in detail elsewhere by Sujata and Jennings [39], does not require the cement samples to be coated with a conductive layer. An accelerating voltage of 15 kV was used for the BEI. As has been noted before [23], this voltage provides good spatial resolution while maintaining good atomic number contrast. A minimum of ten 256 grey-level images of representative paste/aggregate interfaces were captured for each of the mortar and model samples at a magnification of × 500. This magnification results in a resolution of 0.5 μm while also allowing for some averaging of statistical variations in the microstructure.

2.5. Image processing and evaluation

In order to enhance the contrast of the various constituents of the cement system, a grey-level Gaussian filter with a standard deviation of 2.0 was applied to

each grey-level image before analysis. This filter smooths grey-level variations that fall within its deviation limits (noise or statistical variation) while leaving greater variations (atomic number contrast) unchanged. The grey-level histogram was then expanded to make use of all 256 grey levels available for the image. The combined effect of the two techniques is to enhance the peak separation on the grey-level histogram and increase the contrast between the four distinguishable cement components: the anhydrous materials, massive CH, other hydration products (primarily C–S–H), and porosity (see Fig. 3).

Binary images of the anhydrous phase and the porosity phase were created for each captured image by segmenting out that part of the grey-level histogram. Anhydrous material appeared as a distinct peak, easily separated from the remaining histogram. Porosity, however, was not clearly distinguishable from the C–S–H, and the technique first suggested by Scrivener *et al.* [40] had to be used to define the upper grey level for porosity. This method defines the upper grey level for porosity as that point on the histogram where the tangent to the upper portion of the hydration products peak intersects the initial tangent on the grey-level histogram (Fig. 4).

The area percentage, which is representative of the volume fraction of a randomly distributed material, of "on" pixels was measured in 10×500 pixel boxes with the long dimension parallel to the aggregate surface. Each ten pixel width translates to 3.46 μm at a magnification of $\times$ 500. Gradient plots for anhydrous material and pore space were created by plotting the average area percentage versus distance from the aggregate surface of the captured images for each sample (see Figs. 5–8).

3. Results

3.1. Mechanical characterization

The values of compression strength for each limestone mortar mix are shown in Fig. 1 with error bars designating the 90% confidence interval. Comparisons of the strength values between the five mixes reveal that 7 day strengths are largely unaffected by changes in the mixing procedure. At 28 days, strength values exhibit marked, and statistically significant, differences that can be correlated with mixing procedure. Of the five mixes, Mix 1 was designed to have the

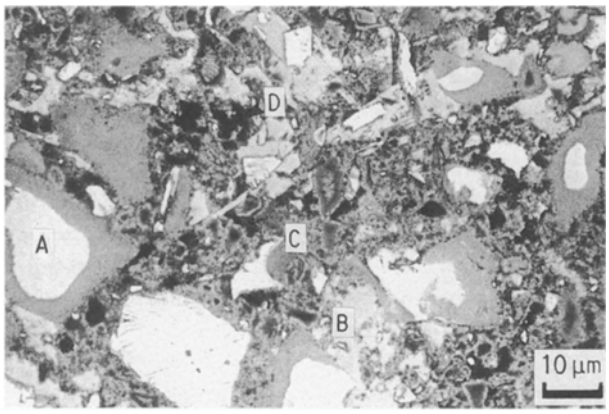

Figure 3 Back-scattered electron micrograph of bulk paste in a limestone mortar. Four distinct phases can be seen: A, anhydrous material; B, calcium hydroxide: C, other hydration products; D, porosity (28 days, w/c/agg = 0.45:1:2.5).

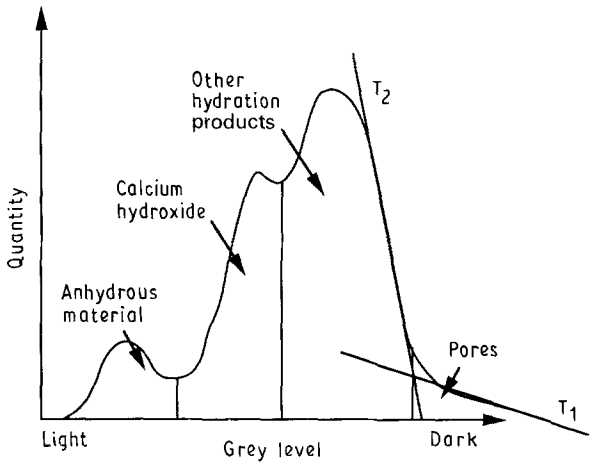

Figure 4 Schematic representation of a typical grey-level histogram for a cement paste. The upper grey level for porosity is defined by the intersection of the initial tangent (T_1) and the tangent to the upper portion of the hydration products peak (T_2).

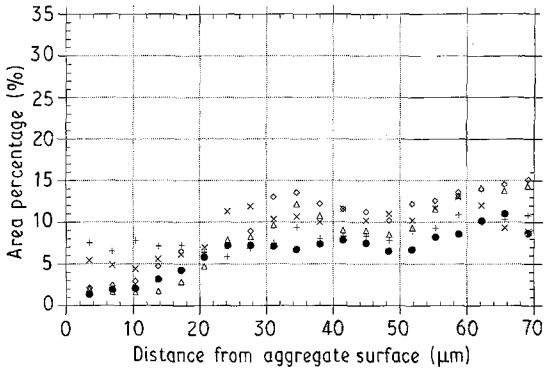

Figure 5 Microstructural gradients in the interfacial region of a limestone mortar. Area percentage of anhydrous material as a function of distance from the interface. Standard error of the mean averaged ± 2–3 area% (7 days). Mix: (●)1, (△) 2, (◇) 3, (×) 4, (+) 5.

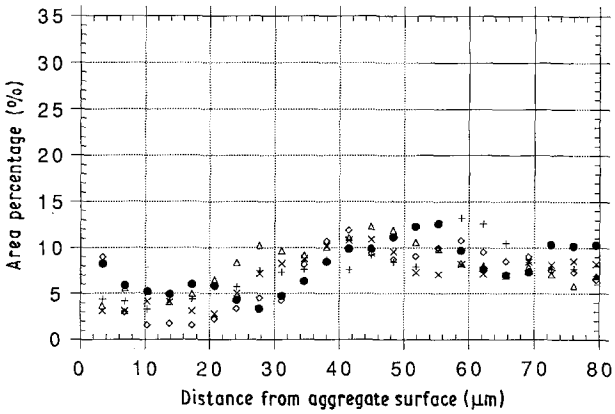

Figure 6 Microstructural gradients in the interfacial region of a limestone mortar. Area percentage of anhydrous material as a function of distance from the interface. Standard error of the mean averaged ± 2–3 area % (28 days). For key, see Fig. 5.

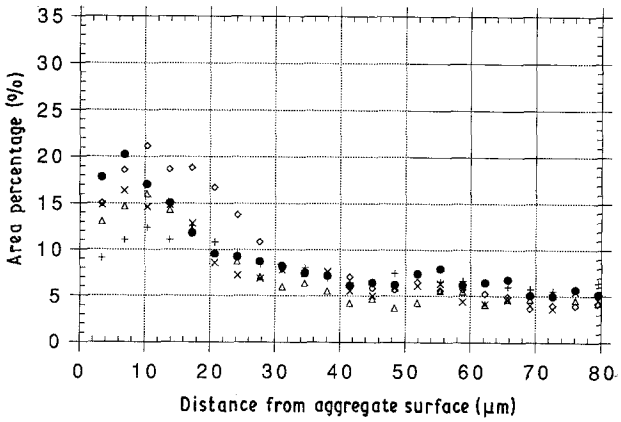

Figure 7 Microstructural gradients in the interfacial region of a limestone mortar. Area percentage of porosity as a function of distance from the interface. Standard error of the mean averaged ± 2–3 area% (7 days). For key, see Fig. 5.

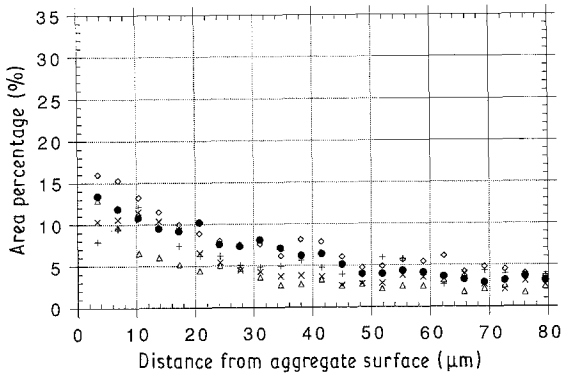

Figure 8 Microstructural gradients in the interfacial region of a limestone mortar. Area percentage of porosity as a function of distance from the interface. Standard error of the mean averaged ± 2–3 area% (28 days). For key, see Fig. 5.

maximum contact between water and aggregate during mixing while the other mixes reduce the water/aggregate contact either by pre-coating or mixing the paste separately. Of the two pre-coat samples, the procedure employing an initial addition of 25% mixing water exhibited the greatest improvements in strength. This result matches those reported by Xueqan *et al.* [31–33] who found optimum strength gains at the same level of initial water contact. The mortars made with paste that was mixed separately (Mixes 4 and 5) also showed significant strength gains at 28 days, although no significant differences were found between these two batches. The results shown in Fig. 1 confirm that significant strength gains can be achieved by reducing the water–aggregate contact and improving the nature of the paste/aggregate bond. Microstructural studies were performed to quantify and characterize these changes, and the data are reported below.

Fracture properties, as determined by the two-parameter fracture model, are presented in Tables VII and VIII. The consistency of the values between the batches and the closeness of the values to those presented previously for other mortars establishes that the model can be used to characterize the fracture properties of the limestone mortars. The high statistical error in these tests, however, prevents any delineation between mixes on the basis of fracture properties at either 7 or 28 days. The model does not appear to be sensitive enough to detect small changes in the mortar system unless a much larger sample population is used. On the basis of average alone, the Young's modulus, the K_{Ic}^{s}, the $CTOD_c$, and the critical crack length, A_c, values follow the trends seen in compression strength. Mixes 2, 4, and 5 exhibit increased Young's modulus values over those of Mix 1. Table VII also includes the critical crack length, a value which can be used as a single expression of the two fracture parameters for a single specimen geometry. Critical crack length values for Mixes 2, 4, and 5 are lower than that of Mix 1. This decrease in critical crack length and increase in Young's modulus implies that these mixes are more brittle than Mix 1. More brittle behaviour implies that better bonding with the aggregate exists and that the aggregate is more closely following traditional composite behaviour by behaving as a reinforcing inclusion rather than merely filler material. Of course, the large statistical error in these results mandates that these observations be treated carefully. Larger sample populations should reduce these errors and will be the focus of future research into microstructure/mechanical property relationships.

3.2. Microstructural characterization

3.2.1. Mortars

Scrivener and Gartner [23] observed that the amount of anhydrous material in the cement paste decreased noticeably as the interface is approached from the bulk paste. Figs 5 and 6 show that the same behaviour was observed in the limestone mortars used in this experiment. Certain general features are observed in all the samples. First, the concentration of anhydrous material rises slowly from about 5 area % at the interface to approximately 10 area % 20–35 μm from the aggregate surface, depending on the sample. BEI also indicates that there is a slight build-up of anhydrous material to concentrations greater than those seen in the bulk paste approximately 30–40 μm from the aggregate surface. The lack of anhydrous material along the interface can be seen in Fig. 9. A large number of Hadley grains are easily visible near this interface, suggesting that only small anhydrous particles are able to pack closely on the surface. Others [7, 23] have noted that small cement particles, typically less than 5 μm in size, hydrate rapidly, often producing Hadley grains. This rapid hydration is most likely due to an increase in the amount of water along the interface.

The effects of the various mixing procedures can be seen in the concentration gradients of anhydrous material in the interfacial zone. This zone is defined as that portion of paste adjacent to the interface where the anhydrous content is below that of the bulk paste. Mix 1, the mortar with maximum water–aggregate contact has the largest interfacial zone, approximately 35 μm at 28 days. Mix 2, the mix with greatest amount of pre-coating, has an average interfacial zone size of

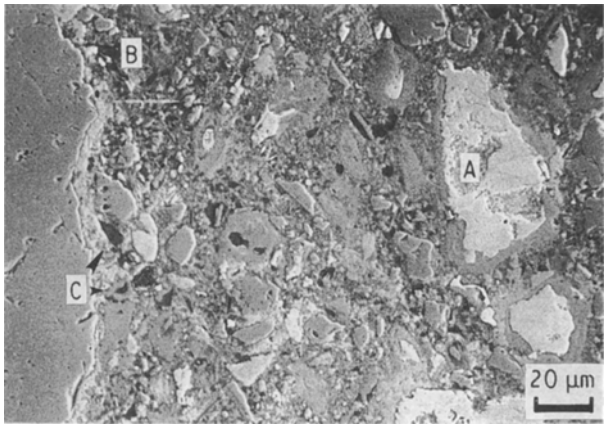

Figure 9 Back-scattered electron micrograph of an interfacial zone in Mix 1. Note the lack of anhydrous material, A, and the high percentage of porosity, B, along the interface. Hadley grains, C, can also be seen in the interfacial zone (28 days, w/c/agg = 0.45:1:2.5).

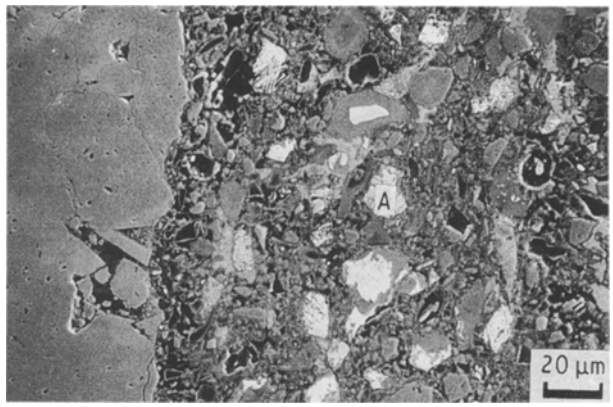

Figure 10 Back-scattered electron micrograph of an interfacial zone in Mix 2. Note the increased percentage of anhydrous material, A, along the interface (28 days, w/c/agg = 0.45:1:2.5).

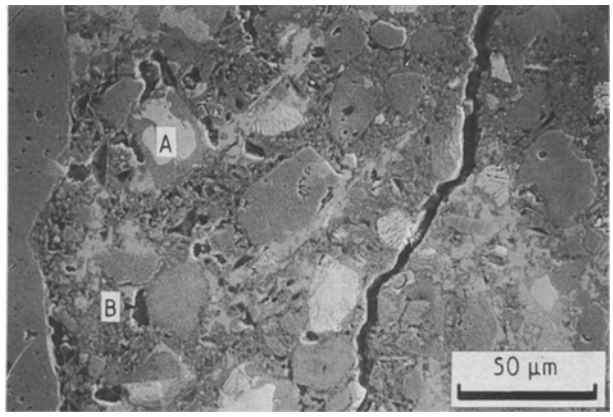

Figure 11 Back-scattered electron micrograph of an interfacial zone in Mix 4. Note the increased percentage of anhydrous material, A, along the interface and the corresponding decrease in porosity, B, (28 days, w/c/agg = 0.45:1:2.5).

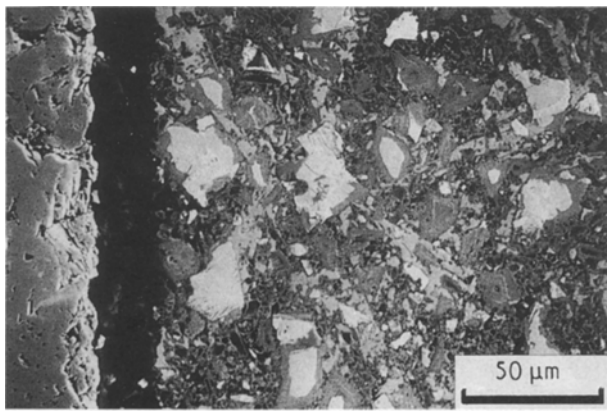

Figure 12 Back-scattered electron micrograph of the interfacial zone of a model interfacial system using cement paste cast against a limestone aggregate. Gap appeared during polishing and is most likely the result of mechanical stresses applied during polishing.

approximately 22 μm, almost one-third less than that of Mix 1. The difference in the size and characters of the two interfacial region can be seen in representative micrographs of the two mortars, Figs 9 and 10. The second pre-coat specimen, Mix 3, has an interfacial zone similar in size and character to Mix 1 at both 7 and 28 days. The similarity of the interfacial zones of Mixes 1 and 3 suggest that the pre-coating process loses its effectiveness at higher initial water concentrations. In mortar made with paste that was mixed separately and then added to the aggregate, the interfacial zone extends approximately 22–25 μm into the bulk cement paste.

Porosity gradients for the five mortar mixes are shown in Figs 7 and 8. In these plots, the interfacial zone is now defined as that portion of paste adjacent to the interface where the porosity concentration is greater than that of the bulk paste. In all the mortars, there is an increase in porosity as the interface is approached from the bulk paste. The largest interfacial zone is found in Mix 1, again indicating that high water concentrations at the aggregate surface enlarge the interfacial zone in mortar and concrete. The sizes of the interfacial zones as determined from the porosity gradients for Mixes 2–5 agree with those determined from the anhydrous gradients.

In mortars where the paste was mixed separately, the curve of porosity versus distance from the interface shows an initial increase in porosity as the interface is approached from the bulk paste, followed by a slight decrease in porosity just before reaching the interface. This curve differs significantly from those reported for the other mortars used in this experiment and those reported elsewhere [23]. The microstructure of a mortar where the paste was mixed separately is shown in Fig. 11, where the high anhydrous and low porosity concentrations along the interface can be seen. No duplex film was seen in any of the mortars.

3.2.2. Model systems

Fig. 12 shows a typical model interface. The gap between the aggregate and the paste appeared during polishing. Because all of the water and ethanol used during sample preparation has been replaced by epoxy and because no epoxy is present in the gap, it is unlikely that drying shrinkage is responsible for the gap. Mechanical stresses, like those applied to the samples during the early steps of polishing (320 and

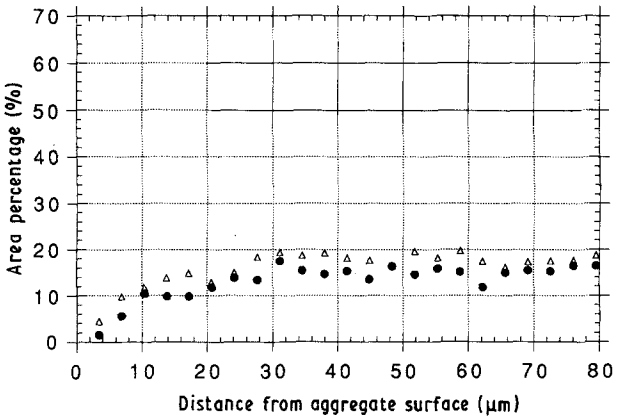

Figure 13 Microstructural gradients in the interfacial region of a model interfacial system using cement paste cast against a limestone aggregate. Area percentage of anhydrous material is shown as a function of distance from the interface. Standard error of the mean averaged ± 2–3 area% (7 days). (●) cast against polished aggregate, (△) mixed with polished aggregate.

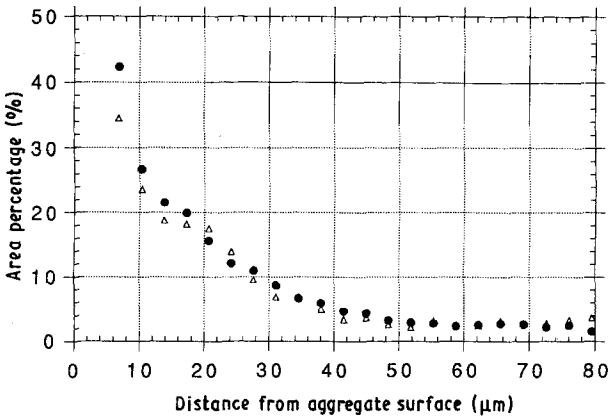

Figure 15 Microstructural gradients in the interfacial region of a model interfacial system using cement paste cast against a limestone aggregate. Area percentage of porosity is shown as a function of distance from the interface. Standard error of the mean averaged ± 2–3 area% (7 days). For key, see Fig. 13.

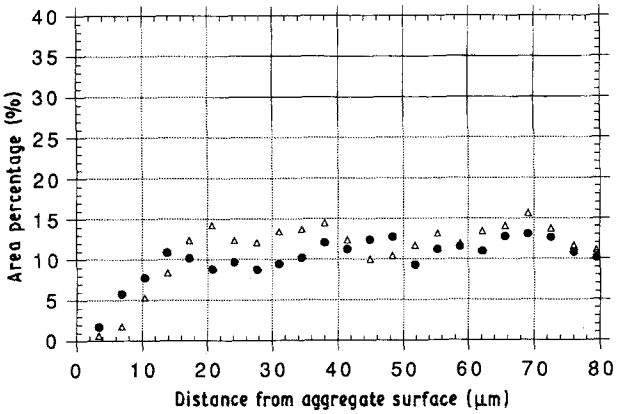

Figure 14 Microstructural gradients in the interfacial region of a model interfacial system using cement paste cast against a limestone aggregate. Area percentage of anhydrous material is shown as a function of distance from the interface. Standard error of the mean averaged ± 2–3 area% (28 days). For key, see Fig. 13.

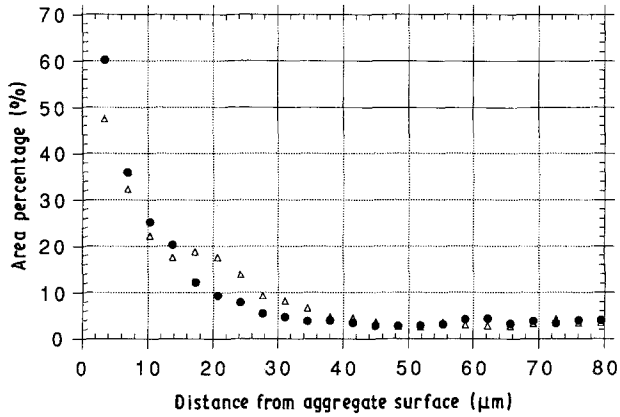

Figure 16 Microstructural gradients in the interfacial region of a model interfacial system using cement paste cast against a limestone aggregate. Area percentage of porosity is shown as a function of distance from the interface. Standard error of the mean averaged ± 2–3 area% (28 days). For key, see Fig. 13.

400 grit paper), most probably separated the paste from the polished surface.

Microstructural gradients in the interfacial zones of the two model systems are shown in Figs 13–16. The shape of the curves agree with those presented in other model studies and those generated by computer simulations [23–41].

4. Discussion

4.1. Mortars

The primary variable in each of the five mixes was the amount and manner in which water came into contact with the aggregate surface. The mechanism by which the precoating procedure reduces the size of the interfacial zone has been discussed by Hayakawa and Itoh [34] and again by Xueqan *et al.* [31–33]. The coating acts to decrease the effective w/c ratio at the interface by coating the particle with a low w/c ratio cement slurry before adding the remainder of the mix water. By reducing the thickness of the water layer that forms on the aggregate surface, anhydrous material packs more tightly against that surface. The combination of these two effects explains the reduction in the interfacial zone size seen in Mix 2 and the corresponding improvements in mechanical properties. The precoating mechanism, however, loses its effect as the initial water concentration increases, resulting in almost identical gradients and similar mechanical properties for Mixes 1 and 3. By mixing the paste separately, as done in Mixes 4 and 5, a better distribution of the cement particles is attained before coming into contact with the aggregate. Also, the mix water is intimately mixed with the cement before contacting the aggregate, reducing the size and effect of any water layers formed at the surface. In turn, capillary porosity is reduced while the increased concentration of anhydrous material at the interface provides a source for the production of space filling C–S–H.

4.2. Open and closed interfaces

Examination of the interfacial microstructure of these five mortar reveals two distinctly different interfaces which have not been defined explicitly in the literature,

hereafter designated "open" and "closed". Open interfaces are like those used for the porosity and anhydrous material gradient analysis. In an open interfacial region, there is significant bulk paste (at least 100–200 μm) adjacent to the interface before another aggregate is encountered. Any variations in porosity, CH, or anhydrous material concentrations along the interface of the aggregate particle can be assumed to be the result of primarily one aggregate. Some inter-aggregate effects may be expected to exist for any interfacial regions, but their relative influence on open interfaces is small.

On the other hand, closed interfaces are those where two or more particles are tightly packed together, leaving only a small ribbon of cement paste, approximately 50–100 μm wide, between the particles. In this case, the assemblage of aggregates influences the microstructure of the ribbon of cement paste, creating a significantly more porous zone that contains a large number of Hadley grains and a large volume of CH. The presence of large volumes of CH reflects the tendency of the mix water to segregate around tightly packed aggregates [22]. Closed interfaces also contain much less anhydrous material than is seen in open interfaces. Large anhydrous grains, in particular, are rarely found in closed interfacial regions. An example of a closed interface is shown in Fig. 17.

Variations in the mixing procedure were found to influence the microstructure of closed interfaces greater than that of open interfaces. As discussed in the gradient analysis above, the interfacial zone of open interfaces was found to decrease in size with changes in water exposure at the aggregate surface. Closed interfaces, however, undergo a more substantial improvement. A comparison of closed interfaces for the various mortar mixes is shown in Figs 17–19. Mix 1 contains highly flawed closed interfaces with massive porosity and CH phases close to the aggregate. Hadley grains are distributed throughout the strip of paste, and very little anhydrous material is present. As the mixing procedure is changed to reduce the water contact with the aggregate, the amount of porosity and CH decreases; moreover, the pre-coating process (Mix 2) and the paste/separate process promote the distribution of anhydrous material into these tight spaces. Mixes 4 and 5 (paste/separate) show dramatic improvement in the microstructure of the closed interfaces (see Fig. 19), implying that incorporation of the mix water into the cement before its addition to the aggregate more evenly distributes cement particles around the aggregate. Massive CH deposits are rarely seen, indicating that this mixing procedure prevents the segregation or bleeding of mix water at the paste/aggregate interface.

These results may help explain the level of improvement in compressive strengths seen in Mixes 2, 4, and 5 at 28 days more than the results documented for open interfaces can. The area percentage of massive porosity seen in closed interfacial regions with BEI is representative of a volume fraction of porosity that extends along the closed interface. Mai and Cotterell have calculated the critical flaw size for mortars to be 1–3 mm [42]. If the massive porosity associated with closed interfaces extends connected or partially connected for closed interfaces, it may act as the critical flaw for initial cracking. Jennings *et al.* and others have suggested that such clusters of porosity may act as the critical flaw and may control fracture and strength properties [7, 42, 43]. Many studies have concluded that cracks to initiate or propagate through interfacial regions [28, 29], but further work is necessary to determine if these closed interfaces act as the

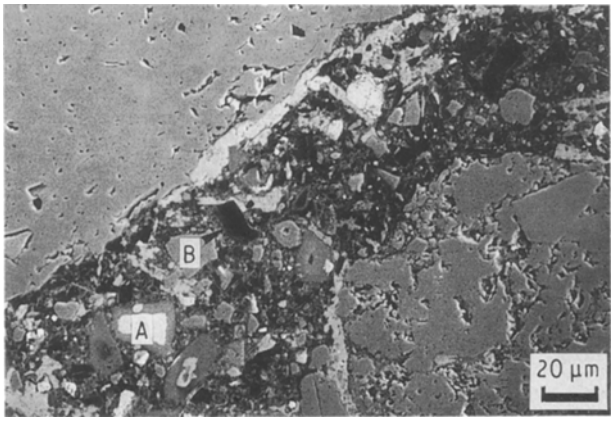

Figure 17 Back-scattered electron micrograph of a closed interface in Mix 1. Note the almost total absence of anhydrous material, A, and the large amount of porosity, B (28 days, w/c/agg = 0.45/1/2.5).

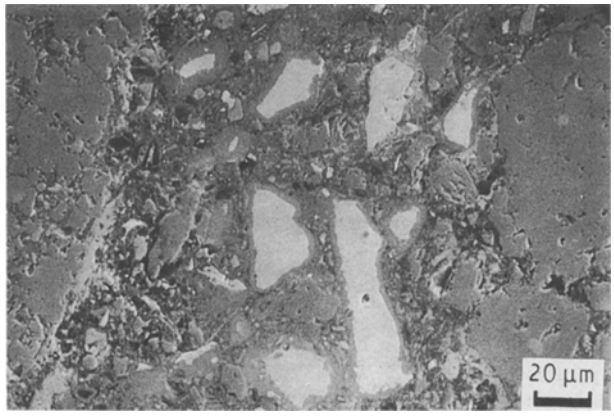

Figure 18 Back-scattered electron micrograph of a closed interface in Mix 2 (28 days, w/c/agg = 0.45/1/2.5).

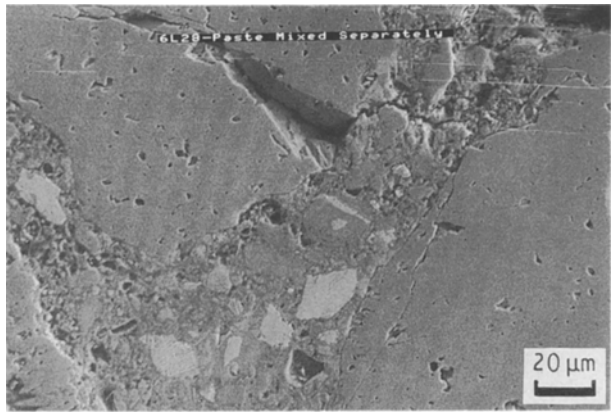

Figure 19 Back-scattered electron micrograph of a closed interface in Mix 4 (28 days, w/c/agg = 0.45/1/2.5).

starting point and controlling variable for crack initiation.

4.3. Model systems

The curves of porosity and anhydrous material versus distance from the interface (see Figs 13–16) vary significantly from those plotted for mortar mixes made with the same aggregate. First, the size of the interfacial region in the model systems is much smaller (10–20 μm) than the size of the interfacial region in mortar systems. Second, the area fraction of porosity in the interfacial zone is much higher in the model materials than in the mortar systems. Thirdly, the area fraction of anhydrous material in the interfacial zone is lower than that seen in the mortar systems. The higher content of porosity and lower content of anhydrous material is most likely due to the formation of a water layer on the polished aggregate surface. The small size of the region compared to those seen in the mortars may be due to the absence of any inter-aggregate effects. Interestingly, no duplex film is seen in either of the model systems (see Fig. 12). The lack of a duplex film may be due to the gap that formed during polishing, or it may simply reflect the absence of the film in these two systems.

The differences between the model and mortar systems emphasize the need to keep model paste/aggregate systems in perspective, both in terms of microstructural and mechanical properties.

5. Conclusions

1. The paste/aggregate bond can be improved by controlling the amount of water that comes into contact with the aggregate during mixing. The interfacial zone of a limestone mortar was reduced in size by controlling the water–aggregate contact through a pre-coating procedure or by mixing the cement paste separately. The pre-coating procedure acts to reduce the size and effect of the water layer which forms on the aggregate surface during mixing by coating the aggregate with a low w/c ratio slurry. Procedures incorporating paste that was mixed separately reduce the water layer by mixing the cement intimately with the water before either comes into contact with the aggregate. This also promotes a better distribution of anhydrous material around the aggregate.

2. Examination of the interfacial microstructure of a mortar reveals that two categories of interfaces exist, "open" and "closed". Open interfaces are those where aggregates are adjacent to a significant amount of bulk paste (100–200 μm). Closed interfaces are those where two or more aggregates are closely packed together, leaving a small ribbon of cement paste (100 μm or less). Closed interfaces appear to contain greater amounts of porosity, CH, and Hadley grains, and smaller amounts of anhydrous material.

3. While both open and closed interfacial regions have improved microstructures when mixed using procedures incorporating pre-coating or mixing the paste separately, the relative improvement in the closed interfacial regions are greater than that for open interfacial regions.

4. Improvements in both compressive strength and fracture properties with improvements in the interfacial microstructure support the view that the paste/aggregate bond is critical to mortar and concrete strength.

5. The size and character of the interfacial zone in model systems differ significantly from that seen in normal mortar systems.

References

1. T. T. C. HSU, F. O. SLATE, G. M. STURMAN and G. WINTER, *J. Amer. Concr. Inst.* **60** (1963) 209.
2. R. L. BERGER, D. S. CAHN and J. D. MCGREGOR, *J. Amer. Ceram. Soc.* **53** (1970) 57.
3. B. PATTEN, UNICIV Report No. R-82, University of New South Wales, Australia (1972).
4. O. VALENTA, in "Prelimenary Report of the International Symposium on the Durability of Concrete", RILEM, Prague, 1961, edited by S. Bechyne and K. Hruban (Czechoslovak Academy of Science, Prague, 1961) p. 53.
5. K. ALEXANDER, J. WARDLAW, and D. J. GILBERT, in "The Structure of Concrete", edited by A. E. Brooks and K. Newman (Cement and Concrete Association, London, 1968) p. 59.
6. L. STRUBLE, in "Materials Research Society Symposium Proceedings", Boston, December 1987, edited by S. Mindess and S. P. Shah, Vol. 114 (Materials Research Society, Pittsburg, PA, 1988) p. 11.
7. S. DIAMOND, in "Proceedings of the 8th International congress on the Chemistry of Cement", Rio de Janeiro, September 1986, Vol. I (Alba Grática e Editora, Rio de Janeiro, 1986) p. 122.
8. J. FARRAN, *Rev. Matér. Constr.* **490–491** (1956) 155.
9. *Idem, ibid.* **492** (1956) 191.
10. J. FARRAN, R. JAVELAS, J. C. MASO, and B. PERRIN, *C. R. Acad. Sci. Ser. D.* **275** (1972) 1467.
11. D. HADLEY, PhD thesis, Purdue University (1972).
12. B. D. BARNES, *Cem. Concr. Res.* **8** (1978) 233.
13. B. D. BARNES, S. DIAMOND and W. L. DOLCH, *J. Amer. Ceram. Soc.* **62** (1979) 21.
14. L. STRUBLE and J. SKALNY, *Cem. Concr. Res.* **10** (1980) 277.
15. P. J. M. MONTEIRO and P. K. MEHTA, *ibid.* **15** (1985) 378.
16. P. J. M. MONTEIRO, J. C. MASO and J. P. OLLIVIER, *ibid.* **15** (1985) 953.
17. J. GRANDET and J. P. OLLIVIER, in "7th International Congress on the Chemistry of Cement", Paris, Vol. 3 (Editions septima, Paris, 1980) pp. VII-63, VII-85.
18. J. C. MASO, *ibid.* Vol. I (1980) pp. VII 1/3-15.
19. A. BENTUR, in "Materials Research Society Symposium Proceedings", Boston, December 1987, edited by S. Mindess and S. P. Shah, Vol. 114 (Materials Research Society, Pittsburg, PA, 1988) p. 133.
20. R. JAVELAS, J. C. MASO, J. P. OLLIVIER and B. THENOZ, *Cem. Concr. Res.* **5** (1975) 285.
21. L. STRUBLE and S. MINDESS, *Int. J. Cem. Comp. Lightw. Concr.* **5** (1983) 79.
22. K. L. SCRIVENER and P. L. PRATT, in "Proceedings of the 8th International Congress on the Chemistry of Cement", Rio de Janeiro, September 1986, Vol. III (Alba Grática e Editora, Rio de Janeiro, 1986) pp. 466–71.
23. K. L. SCRIVENER and E. M. GARTNER, in "Materials Research Society Symposium Proceedings", Boston, December 1987, edited by S. Mindess and S. P. Shah, Vol. 114 (Materials Research Society, Pittsburg, PA, 1988) p. 77.
24. J. GRANDET and J. P. OLLIVIER, in "7th International Congress on the Chemistry of Cement", Paris, Vol. III (Editions septima, Paris, 1980) pp. VII-85.
25. R. J. DETWILER, P. J. M. MONTEIRO, H. R. WENK, and Z. ZHONG, *Cem. Concr. Res.* **18** (1988) 823.
26. E. GARTNER, *Adv. Cem. Res.* **2** (6) (1989) 79.

27. K. L. SCRIVENER, A. BENTUR and P. L. PRATT, *ibid.* **1** (4) (1988) 230.
28. S. MINDESS and S. DIAMOND, *Cem. Concr. Res.* **12** (1982) 569.
29. A. MAJI and S. P. SHAH, in "Materials Research Society Symposium Proceedings", Boston, December 1987, edited by S. Mindess and S. P. Shah Vol. 114 (Materials Research Society, Pittsburg, PA, 1988) p. 55.
30. A. GOLDMAN and A. BENTUR in "Microstructure, Interfacial Effects and Micromechanics of Cementitious Composites", quoted by A. Bentur, in "Ceramic Transactions, Advances in Cementitious Materials", edited by S. Mindess Vol. 14 (American Ceramic Society, Westerville, OH, 1991) p. 523.
31. W. XUEQAN, H. SUFEN, B. QINGHAN and T. MINGSHU, in "Proceedings of the 8th International Congress on the Chemistry of Cement", Rio de Janeiro, September 1986, Vol. III (Alba Grática e Editora, Rio de Janeiro, 1986) pp. 454–9.
32. W. XUEQAN, L. DONGXU, B. QINGHAN, G. LIQUN and T. MINGSHU, *Cem. Concr. Res.* **17** (1987) 709.
33. W. XUEQAN, L. DONGXU, W. XIUN and T. MINGSHU, in "Materials Research Society Symposium Proceedings", Boston, December 1987, edited by S. Mindess and S. P. Shah, Vol. 114 (Materials Research Society, Pittsburg, PA, 1988) p. 35.
34. M. HAYAKAWA and Y. ITOH, in "Bond in Concrete", edited by P. Bartos (Applied Science, London, 1985) p. 282.
35. Y. HIGUCHI, *Concr. Int.* **2** (5) (1980) 75.
36. Y. JENQ and S. P. SHAH, *J. Eng. Mech. Div. ASCE* **111** (1985) 1227.
37. RILEM Recommendation, *Materials and Structures* **23** (1991) 457.
38. L. STRUBLE and P. STUTZMAN, NBS Report NBSIR 88–3702 (1988).
39. K. SUJATA and H. M. JENNINGS, *MRS Bull.* **16** (3) (1991) 41.
40. K. SCRIVENER, H. H. PATEL, P. L. PRATT and L. J. PARROTT, in "Materials Research Society Symposium Proceedings", Boston, December 1986, edited by L. J. Struble and P. W. Brown Vol. 85 (Materials Research Society, Pittsburg, PA, 1987) p. 67.
41. D. P. BENTZ and E. J. GARBOCZI, *J. Mater. Res.* **6** (1991) 196.
42. H. M. JENNINGS, L. J. STRUBLE, J. R. CLIFTON, and G. FROHNSDORFF, in "Proceedings of the First NCB International Seminar on Pragmatic Strategies for Productivity and Modernisation", New Delhi, 1987, Vol. 4 (National Council for Cement and Building Materials, New Delhi, 1987) p. IX–1–8.
43. Y. W. MAI and B. COTTERELL, *Cem. Concr. Res.* **15** (1985) 995.

Received 2 September 1991
and accepted 17 February 1992